JOURNAL OF GEOPHYSICAL RESEARCH, VOL. 106, NO. B7, PAGES 13,739–13,750, JULY 10, 2001

Fault slip rates and initiation age based on diffusion equation modeling: Wasatch Fault Zone and eastern Great Basin

Ann Mattson and Ronald L. Bruhn

Department of Geology and Geophysics, University of Utah, Salt Lake City, Utah

Abstract. Models of the evolution of fault scarp morphology provide time elapsed since slip initiated on a faulted surface and may therefore provide more accurate estimates of slip rate than the rate calculated by dividing scarp offset by the age of the ruptured surface. To accomplish this task, linear and nonlinear models of sediment transport are calibrated from the morphology of Lake Bonneville shoreline scarps and fault scarps formed by multiple, surface-rupturing earthquakes along the Wasatch Fault Zone (WFZ). Profile modeling of scarps formed by several events distributed through time is done using a constant slip rate (CSR) solution and yields a value of A/κ (1/2 slip rate/diffusivity). Time elapsed since slip initiated on a fault is determined by establishing a value for κ and measuring total scarp offset. CSR nonlinear modeling ($\kappa_0 = 2.8 \pm 1.1$ m^2/kyr, WFZ) of faults along the west slope of the Oquirrh Mountains indicates a slip rate of ~0.1 mm/yr since 50 to 65 ka, which is corroborated by cosmogenic dating (^{10}Be / ^{26}Al age = 75 ka). The slip rate along the west flank of the Stansbury Mountains varies from 0.04 to 0.2 mm/yr for time frames of 10 to >100 ka, with the most recent rupture on the northern portion of the fault zone ~10 ka. Scarp analysis of the southern end of the Nephi segment, WFZ, suggests either temporal clustering or variable slip rate as indicated by differences in the short-term (1.3 mm/yr for 4.3 ka) versus long-term (0.4 mm/yr for 70 ka) slip rates.

1. Introduction

Fault slip rate and temporal pattern of faulting are two critical tectonic parameters that influence landscape evolution and are of interest for seismic hazard assessment [*McCalpin*, 1996; *Keller and Pinter*, 1996]. Slip rate determines how rapidly geological features are offset by faulting, and the temporal pattern of faulting determines how rupturing repeats through time. The evolving morphology of fault scarps is a fundamental geologic feature of a tectonically active landscape. Diffusion equation modeling relies on the evolution of scarp morphology to estimate fault slip rate and the elapsed time since slip initiated. This method provides a quick and inexpensive way to gather data for a regional tectonic study and for estimating relative rates of tectonic activity.

Most previous applications of diffusion equation modeling determined the age of the last surface-rupturing event [*Bucknam and Anderson*, 1979; *Nash*, 1984; *Hanks et al.*, 1984; *Mayer*, 1984; *Hanks and Wallace*, 1985; *Bowman and Gerson*, 1986; *Hanks and Schwartz*, 1987; *Enzel et al.*, 1996; *Arrowsmith et al.*, 1998], but a few studies used fault scarp morphology to infer long-term slip rates or the temporal pattern of faulting [*Hanks et al.*, 1984; *Tapponnier et al.*, 1990; *Avouac and Peltzer*, 1993]. Most of these studies relied on fluvial, lacustrine, or marine terraces of known age to calibrate the diffusion parameters [*Bucknam and Anderson*, 1979; *Nash* 1980; *Hanks et al.*, 1984; *Nash*, 1984; *Hanks and Wallace*, 1985; *Pierce and Colman*, 1986; *Andrews and Bucknam*, 1987; *Hanks and Andrews*, 1989; *Avouac and Peltzer*, 1993; *Avouac et al.*, 1996; *Hanks*, 1999]. Early empirical regression methods plotted scarp height versus maximum slope angle to estimate the age of the scarp [e.g., *Bucknam and Anderson*, 1979], but more recent methods match a suite of calculated topographic profiles to field measurements [e.g., *Mayer*, 1984; *Avouac et al.*, 1993; *Arrowsmith et al.*, 1998]. The latest advancement is to implement nonlinear sediment transport models as opposed to linear transport models [*Andrews and Bucknam*, 1987; *Hanks and Andrews*, 1989; *Roering et al.*, 1999; D.J. Andrews and T.C. Hanks, Diffusive evolution of hillslopes toward dynamic equilibrium, submitted to *Journal of Geophysical Research*, 2000, hereinafter referred to as Andrews and Hanks, submitted manuscript, 2000]. These nonlinear models incorporate the frictional characteristics of granular aggregates and generally reproduce field morphology more accurately than linear models.

Topographic profiles of Lake Bonneville shoreline scarps have been used to calibrate the single-event, diffusion equation [*Bucknam and Anderson*, 1979; *Hanks et al.*, 1984; *Andrews and Bucknam*, 1987; *Hanks and Andrews*, 1989], but the wealth of paleoseismology data for the Wasatch Fault Zone (WFZ) has not been utilized until now. Paleoseismology trenches have been excavated at 14 sites along the central five segments of the WFZ in an effort to characterize the slip rate and recurrence interval of surface-rupturing events since 10 ka (1 ka = 1000 calendar years before present) [*McCalpin and Nishenko*, 1996]. These studies compile age and rupture offset data for each event and provide a database to use as input to calibrate the parameters in the diffusion equation. WFZ trench studies provide rupture histories for three to five events since 10 ka, but solutions to the diffusion equation can be used to estimate longer-term slip rates from older scarps formed by earlier surface-rupturing events.

First, our paper discusses the linear and nonlinear sediment transport models, the incorporation of these transport models into the diffusion equation, and the various solutions to the diffusion

Paper number 2001JB900003.
0148-0227/01/2001JB900003$09.00

equation. Next, we will describe calibration of the parameters for the linear and nonlinear diffusion equation using Lake Bonneville shoreline scarps and multiple-event fault scarps from the WFZ. Finally, we will apply the nonlinear solution to undated fault scarps along the WFZ and in the eastern Great Basin to estimate temporal and spatial variations in slip rates and time elapsed since slip initiated.

2. Models

Successful application of the morphological dating method requires selection of an appropriate sediment transport model and calibration of the associated parameters. Sediment transport models are either linear or nonlinear, and diffusivity and critical slope are parameters of the aggregate sediment. Three different solutions for each transport model are applied depending on the assumed temporal rupture pattern that generated the scarp: single-event (SE), multiple-event (ME), or constant slip rate (CSR). "Single-event" scarps are formed at a unique point in time, i.e., one surface-rupturing earthquake, a rapid drop in lake level, or lateral stream erosion of a terrace riser. "Multiple-event" scarps are formed as the result of several discrete, surface-rupturing events. "Constant slip rate" refers to the approximation of a multiple-event scarp by accumulating surface offset at a constant rate. The CSR method is used when the rupture history is not known or when the history exceeds that determined by trenching.

The implementation of one-dimensional diffusion equation models requires several assumptions. (1) A scarp forms by rupturing unconsolidated material. (2) Sediment transport is controlled by diffusive processes such as rain splash and soil creep. (3) Mass is conserved as material is transported from the crest to the base of the scarp. (4) The fault ruptures the surface at the same point each time. (5) The diffusivity constant is independent of time [*Buchun et al.*, 1986; *Hanks*, 1999]. The diffusivity constant can also be thought of as the "time-averaged" diffusivity for a particular time period. The linear diffusion equation model assumes that sediment flux is proportional to topographic gradient (Figure 1). The nonlinear diffusion equation model assumes sediment flux is proportional to gravity and other driving forces and resisted by the intergranular friction of the soil. The SE and ME modeling methods also assume that degradation of the scarp from an initial, steep free face (60°-90°) to an angle of repose (35°-40° for poorly sorted angular materials [*Terzaghi*, 1950]) represents a short period of time (tens to hundreds of years) relative to the total elapsed time (thousands of years). The initial condition for SE and ME profiles is a scarp at the angle of repose. The initial condition for CSR profiles is a planar surface with no offset.

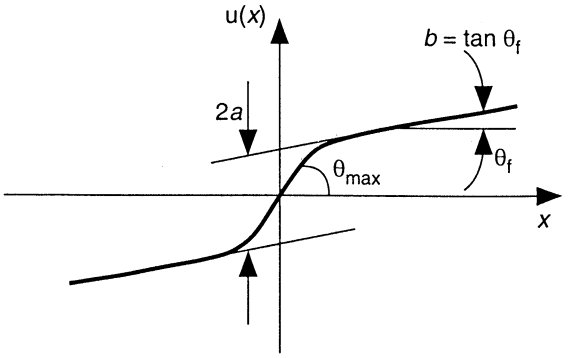

Figure 1. Geometry of a scarp profile indicating geometrical parameters.

2.1. Sediment Transport Models

Scarp degradation can be expressed as a differential equation that combines a continuity equation (conservation of mass) with a sediment transport model. The governing diffusion equation is

$$\frac{\partial u}{\partial t} = \frac{\partial}{\partial x}\left[F\left(\frac{\partial u}{\partial x}\right)\right], \tag{1}$$

where u is elevation, x is horizontal distance, and t is time. F represents the transport of material at any point along a profile and is a function of the slope of the profile, $\partial u/\partial x$. The linear sediment transport model is defined by a constant diffusivity (κ) times the topographic gradient:

$$F\left(\frac{\partial u}{\partial x}\right) = \kappa\frac{\partial u}{\partial x}. \tag{2}$$

The nonlinear sediment transport model is defined as diffusivity at small slope (κ_0) times a function of topographic gradient and critical slope (S_c):

$$F\left(\frac{\partial u}{\partial x}\right) = \kappa_0\frac{\partial u/\partial x}{1-\left(\frac{\partial u/\partial x}{S_c}\right)^2}. \tag{3}$$

The nonlinear transport model (3) is the frictional sliding model of *Andrews and Bucknam* [1987]. This model assumes that particle movement is controlled by its initial velocity, gravity, and friction and that a particle can be disturbed by driving forces to slide either up or down a slope until it comes to rest. The amount of material transported approaches infinity as the profile slope approaches S_c [*Roering et at.*, 1999; Andrews and Hanks, submitted manuscript, 2000]. The critical slope is also equivalent to the coefficient of friction for the sediment. This nonlinear transport model reduces to the linear transport model for small slopes.

Diffusion equation models are represented by the following partial differential equations that are found by combining the general diffusion equation model (1) with the linear (2) and nonlinear (3) transport models:

$$\frac{\partial u}{\partial t} = \kappa\frac{\partial^2 u}{\partial x^2} \tag{4}$$

$$\frac{\partial u}{\partial t} = \frac{\kappa_0\frac{\partial^2 u}{\partial x^2}}{1-\left(\frac{\partial u/\partial x}{S_c}\right)^2}\left[1+\frac{2\left(\frac{\partial u}{\partial x}\right)^2}{S_c^2\left[1-\left(\frac{\partial u/\partial x}{S_c}\right)^2\right]}\right]. \tag{5}$$

2.2. Numerical Versus Analytical Solutions

In this study we implement forward numerical solutions to (4) and (5) and analytical solutions to (4). Forward numerical methods implement SE, ME, or CSR initial conditions and use discrete increments in space and time to build scarp profiles. The SE and ME modeling approaches begin with a preexisting surface that ruptures, reaches the angle of repose, and then degrades for a period of time. The SE history is complete after the degradation of the one-event scarp. The ME history, however, simulates a sequence of rupture events with each rupture

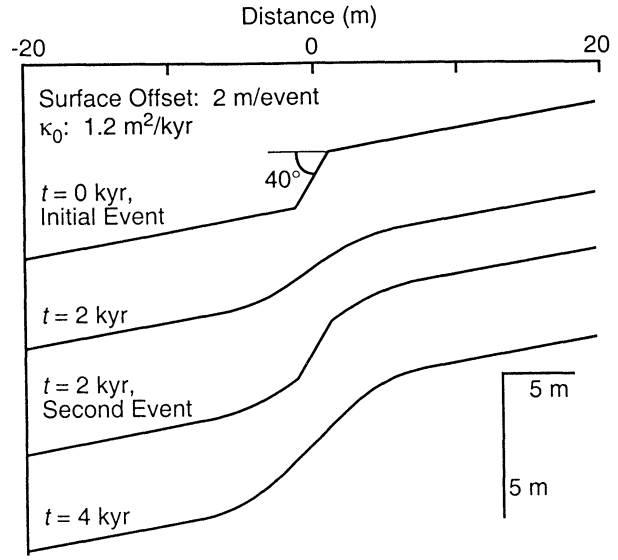

Figure 2. Procedure to build a fault scarp profile that records two surface-rupturing seismic events. The rupture history is known from paleoseismic trench data, and diffusivity is calibrated for the study area. The initial scarp angle is assumed to be 40°, i.e., the angle of repose for angular, poorly sorted materials.

separated by a period of quiescence during which the scarp degrades (Figure 2). The CSR modeling approach simulates incremental offset of a geomorphic surface at a constant rate. Incremental offsets are <1 mm and are deemed sufficiently small to allow us to ignore the angle of repose when applying a CSR solution. The scarp continuously degrades as offset accumulates.

Analytical solutions exist for the SE and CSR linear diffusion equation (4) [*Hanks et al.*, 1984] but do not exist for the nonlinear diffusion equation (5) [*Hanks*, 1999]. To apply the analytical solution, the inflection point of the field profile must be shifted to the axis origin (Figure 1). The SE analytical solution for linear diffusion is solved for κt (diffusivity times elapsed time):

$$u(x,t) = a\,\mathrm{erf}\left(x/2\sqrt{\kappa t}\right) + bx\,. \tag{6}$$

The constants a and b are half the scarp offset and far-field slope, respectively, and erf is the error function. The CSR analytical solution is solved for A/κ (half slip rate divided by diffusivity):

$$u(x,t) = (a + At)\,\mathrm{erf}\left(\frac{x}{2\sqrt{\kappa t}}\right) + \frac{Ax^2}{2\kappa}\left[\mathrm{erf}\left(\frac{x}{2\sqrt{\kappa t}}\right) - \mathrm{sgn}(x)\right] + \frac{Ax}{\kappa}\sqrt{\frac{\kappa t}{\pi}}\,e^{\left(-x^2/4\kappa t\right)} + bx\,. \tag{7}$$

The sign function, sgn, returns +1 or −1 based on the sign of the argument. During calibration, profile curves generated by both linear and nonlinear transport models are matched to the field data. Because of differing initial conditions, calibrated parameters are not interchangeable between models, but the best fit curves generated by each model are similar.

3. Data Collection

Scarp profiles were surveyed with either a total station or a laser range finder. Horizontal and vertical errors are estimated to be a few centimeters. The laser range finder became the instrument of choice due to ease of use and portability; the better resolution of the total station was deemed unnecessary. Several profiles were surveyed at all sites except Kaysville to quantify profile variability along a scarp. Much of the data along the Stansbury Mountains was previously collected by *Helm* [1995] using an Abney level and tape.

Diffusion equation profile curves are generated to match the upper half of a field profile [Hanks and Schwartz, 1987]. The lower half of a scarp profile is usually rejected because it may be modified by lateral sediment transport, sediment ponding in a graben, or back rotation of the hanging wall into the fault. The relative misfit between the model data elevation (um_i) and the field data elevation (uf_i) is measured using the standard deviation (σ) for the total number of profile points (N):

$$\sigma = \left[\frac{1}{N}\sum_{i=1}^{N}(uf_i - um_i)^2\right]^{1/2}. \tag{8}$$

The minimum σ corresponds to the "best fit" κt for the SE and ME solutions and A/κ for the CSR solution.

The linear model requires the calibration of only one parameter, κ, but the nonlinear model requires optimization of two parameters, κ_0 and S_c. S_c ranges between 0.75 and 1.4 according to the results of *Andrews and Bucknam* [1987], *Roering et al.* [1999], and Andrews and Hanks (submitted manuscript, 2000) but is probably <1 for unconsolidated alluvium.

Table 1. UTM Zone 12N Coordinates of Profile Locations

Site	Easting, m	Northing, m
Fault calibration		
Brigham City	416700	4597050
East Ogden	421900	4566450
Kaysville	424600	4541400
American Fork	436350	4475400
Nephi	429200	4399000
Levan	421050	4363600
Shoreline calibration		
North Ogden	419100	4575950
South Willow Canyon	372000	4487000
Tooele	387600	4482900
Stansbury Mountains		
Broon Canyon	359000	4496250
North Big Creek	355100	4483700
South Big Creek	355000	4483000
Fault application		
North Oquirrh	394800	4502150
Mercur	392000	4461750
Box	360450	4492300
Little Granite	360600	4491100
Monument	360500	4489700
Round/Box	360400	4492950
North Pass	358800	4487400
South Big Pole Fan	357500	4485000
North Spring	357300	4484300
South Big Creek	356800	4482600
North North Lost Creek	356700	4481200
South North Lost Creek	356800	4480800
South South Lost Creek	356900	4479300
North Antelope Indian Hickman	357800	4476000
South Antelope Indian Hickman	357800	4475600

4. Calibration of Model Parameters

Diffusivity is calibrated for the linear and nonlinear diffusion equation using SE, ME, and CSR solutions. Lake Bonneville shoreline scarp profiles (Table 1 and Figure 3) are used to calibrate diffusivity for the SE solution and to determine S_c for alluvial fan materials. The age of Lake Bonneville shoreline scarps is 14.5 ka ^{14}C or ~17 ka (D. M. Currey, personal communication, 1998). Fault scarps created by multiple surface-rupturing events (Table 1 and Figure 3) are used to calibrate diffusivity for the ME and CSR solutions. The offset and age of surface-rupturing events are provided by paleoseismology trench studies along the WFZ [*Jackson*, 1991; *Personius*, 1991; *Forman and Nelson*, 1991; *McCalpin et al.*, 1994]. These studies utilize ^{14}C and thermoluminescence (TL) techniques to date material in colluvial wedges or to date ruptured geomorphic surfaces that bracket the age of an event. Diffusivity for the ME solution is calibrated using offset and age data for each event in the paleoseismic history at the site. Diffusivity for the CSR solution is calibrated using total scarp offset and the age of the oldest event at the site.

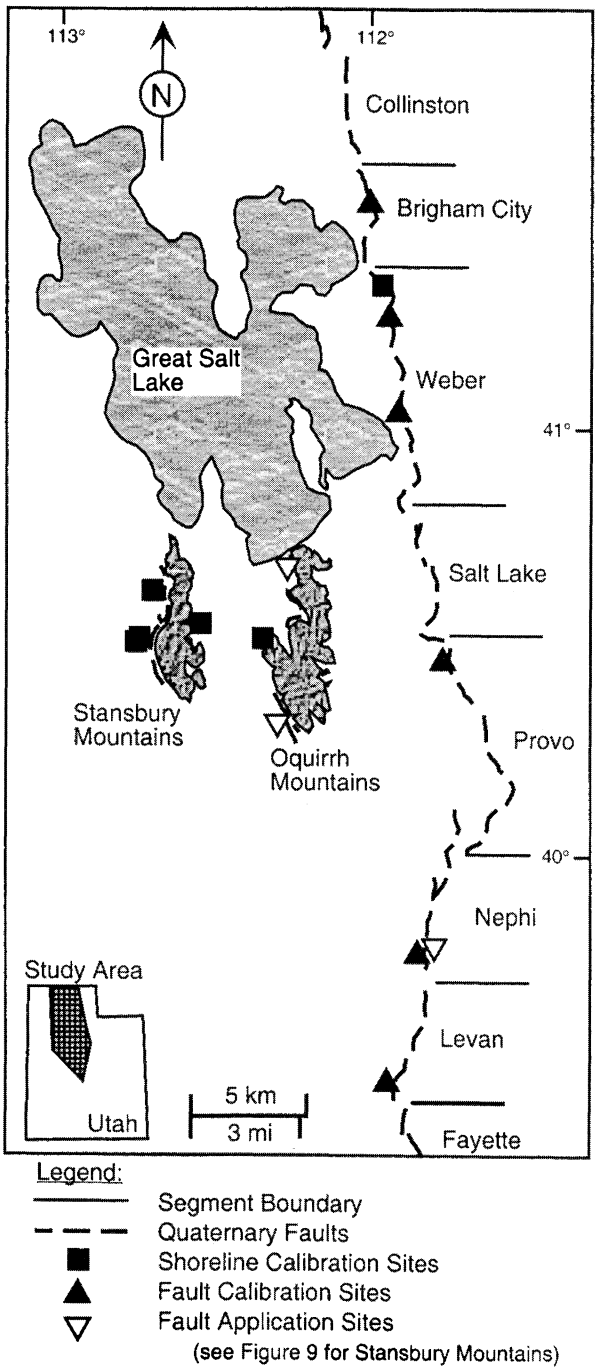

Figure 3. Location map for the eastern Great Basin indicating Quaternary faults involved in this study, WFZ segment boundaries, calibration sites for Lake Bonneville shoreline scarps and WFZ scarps, and application sites along the Wasatch and Oquirrh Mountains. Application sites for the Stansbury Mountains are shown on Figure 9. Geographic coordinates for profiles at each site are listed in Table 1.

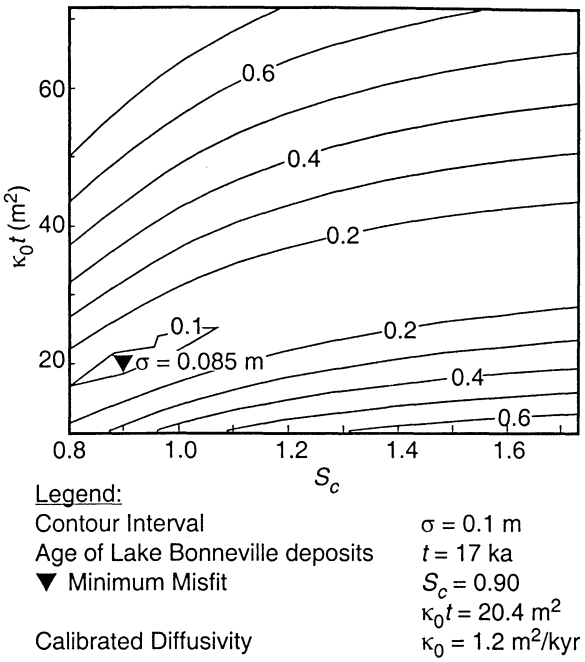

Figure 4. Plot of σ (standard deviation) as a function of $\kappa_0 t$ (diffusivity times elapsed time) and S_c (critical slope) for a Lake Bonneville shoreline scarp near the mouth of South Willow Canyon. The preferred $\kappa_0 t$ solution corresponds to the minimum standard deviation. The Lake Bonneville flood occurred at 17 ka, and therefore κ_0 can be calculated.

4.1. Lake Bonneville Shoreline Scarps

Lake Bonneville shoreline scarps can serve as a proxy for SE fault scarps because Lake Bonneville broke through a natural dam in the northeast part of the basin and the level dropped ~100 m in as little as a few weeks. Shoreline scarps are particularly useful for comparing linear and nonlinear model profiles. The linear model is calibrated for κ, and the nonlinear model is calibrated for S_c and κ_0 (Figure 4). The average S_c found from the shoreline scarps is 0.95 ± 0.08 and was used in all subsequent nonlinear models. All uncertainties in this paper are reported as one standard deviation on either side of the mean.

Best fit SE nonlinear profiles are shown with the field data in Figure 5, and the results indicate the value for κ_0 is usually about half the value of κ (Table 2). The κ correlates positively with scarp height for scarps more than 15–20 m tall [*Hanks et al.*, 1984; *Pierce and Colman*, 1986; *Andrews and Bucknam*, 1987], but for κ_0 the effect is limited to scarps more than 25 m tall (Figure 6). This relationship may be due to nondiffusive scarp

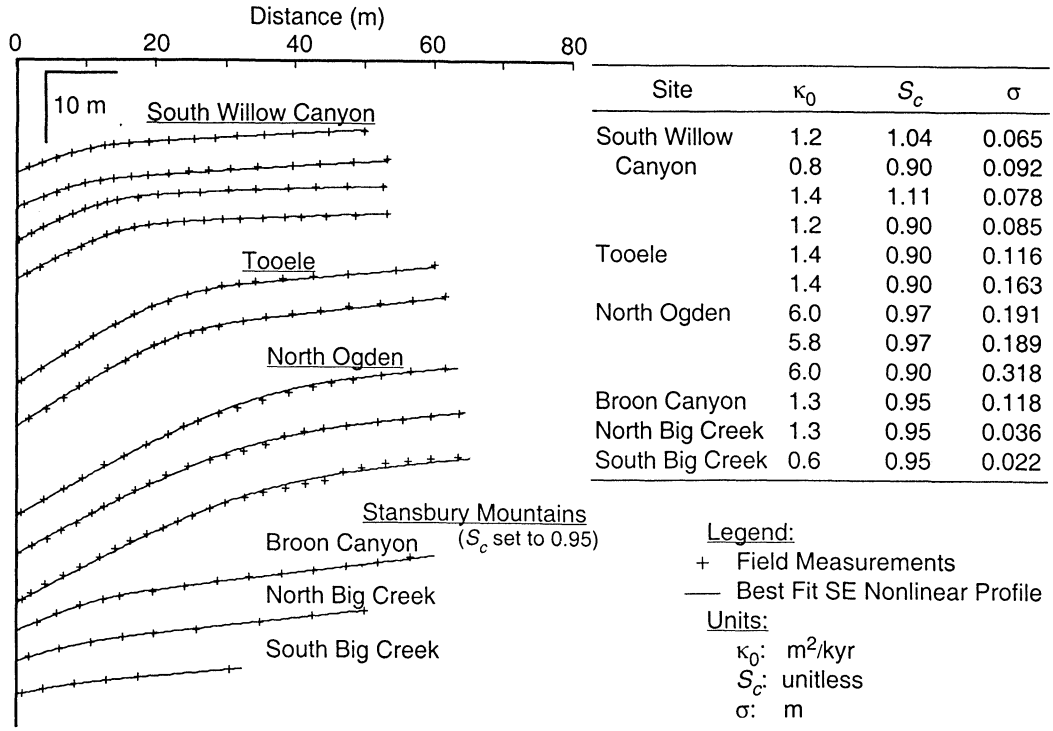

Site	κ_0	S_c	σ
South Willow	1.2	1.04	0.065
Canyon	0.8	0.90	0.092
	1.4	1.11	0.078
	1.2	0.90	0.085
Tooele	1.4	0.90	0.116
	1.4	0.90	0.163
North Ogden	6.0	0.97	0.191
	5.8	0.97	0.189
	6.0	0.90	0.318
Broon Canyon	1.3	0.95	0.118
North Big Creek	1.3	0.95	0.036
South Big Creek	0.6	0.95	0.022

Figure 5. Upper half of Lake Bonneville shoreline scarp profiles for calibration sites in the eastern Great Basin (Table 1). To the right of the profiles κ_0, S_c, and σ are shown for each best fit profile. The average S_c calibrated from these profiles (excluding scarps from the Stansbury Mountains) was used in fault scarp calibration.

degradation processes, such as slumping or creep, that tend to be more pronounced on taller scarps and result in excess sediment transport. For example, κ_0 is found to be 5.9 m²/kyr for 30 m tall scarps at North Ogden , ~5 times greater than κ_0 for other shoreline scarps, 1.2 m²/kyr. These North Ogden scarps exhibit hummocky topography that is usually associated with slumping or creep. *Andrews and Bucknam* [1987] and *Hanks and Andrews* [1989] found no correlation between κ_0 and scarp height for the nonlinear model for scarps 1-12 m tall.

4.2. Multiple-Event Fault Scarps

"Best fit" profiles based on the ME and CSR nonlinear solutions are compared to field profiles for each calibration site along the WFZ (Figure 7). Elapsed time is known from trench data, and diffusivity (Table 3) is determined from the minimum misfit result (Figure 8). Diffusivity values for the ME nonlinear solution calibrated from fault scarp profiles are comparable to diffusivity values for the SE nonlinear solution calibrated from shoreline scarp profiles. There is no correlation between diffusivity and scarp height for the fault scarps used in calibration (Figure 6).

Diffusivities (κ_0 and κ) calibrated for profiles measured at the Brigham City site are ~2 times greater than the next largest value found in this study. The reason for this discrepancy is not obvious since the scarp offsets are relatively small (~5 m). Possible explanations for this high diffusivity value include excess sediment transport due to steep far field slopes (14°) above the scarps, slumping of scarp faces prior to degradation, underestimating the age of the oldest rupture event, and modification of the area by development.

The fit of ME nonlinear profiles to the field data (σ = 0.08 ± 0.04 m) is similar to CSR nonlinear profiles (σ = 0.09 ± 0.04 m). Therefore the CSR nonlinear solution can be used to approximate fault scarp evolution in areas without independent age data for the elapsed time in the calibration exercise, <10 kyr. Over longer time periods, the agreement between these models may diverge.

Table 2. Summary of Lake Bonneville Shoreline Calibration Sites

Site	Number of Profiles	Height, m	S_c	κ_0 SE, m²/kyr	κ SE, m²/kyr
North Ogden	3	29.5 ± 2.7	0.94 ± 0.04	5.9 ± 0.1	12.9 ± 1.7
South Willow Canyon	4	10.1 ± 3.9	0.99 ± 0.10	1.2 ± 0.3	1.9 ± 0.5
Tooele	2	23.1	0.97	1.4	4.7
Stansbury Mountains	3	4.2 ± 2.9	NA*	1.1 ± 0.4	1.8 ± 0.9
Average			0.95 ± 0.08	2.4 ± 2.2	5.1 ± 4.9
Average without North Ogden			0.96 ± 0.09	1.2 ± 0.3	2.5 ± 1.4

*NA, not available.

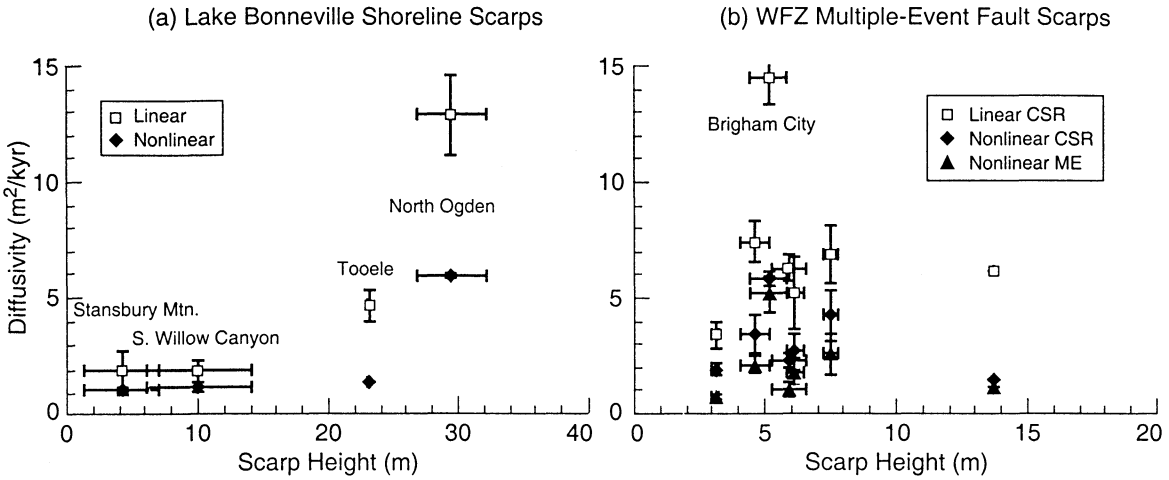

Figure 6. Diffusivity for linear and nonlinear transport laws as a function of scarp height: (a) Lake Bonneville shoreline scarps; (b) WFZ multiple-event fault scarps. The results from the WFZ do not indicate a correlation between diffusivity and scarp height, but the results from the Lake Bonneville shoreline scarps do indicate a positive correlation for scarps more than 20–30 m high. This effect is more pronounced for the linear sediment transport model than for the nonlinear sediment transport model.

4.3. Guidelines to Application of Diffusion Models

Evaluation of tectonic activity based on fault scarp morphology requires choosing an appropriate sediment transport model and the solution to that model and assigning values to the model parameters. Standard deviation between model and field profiles for the linear and nonlinear sediment transport models does not vary significantly (Lake Bonneville shoreline scarps: $\sigma_{linear} = 0.12$ m; $\sigma_{nonlinear} = 0.14$ m). Therefore the nonlinear model is preferred because there is less correlation between κ_0 and scarp height ($2a < 25$ m).

For scarps formed by a single surface-rupturing event, the SE

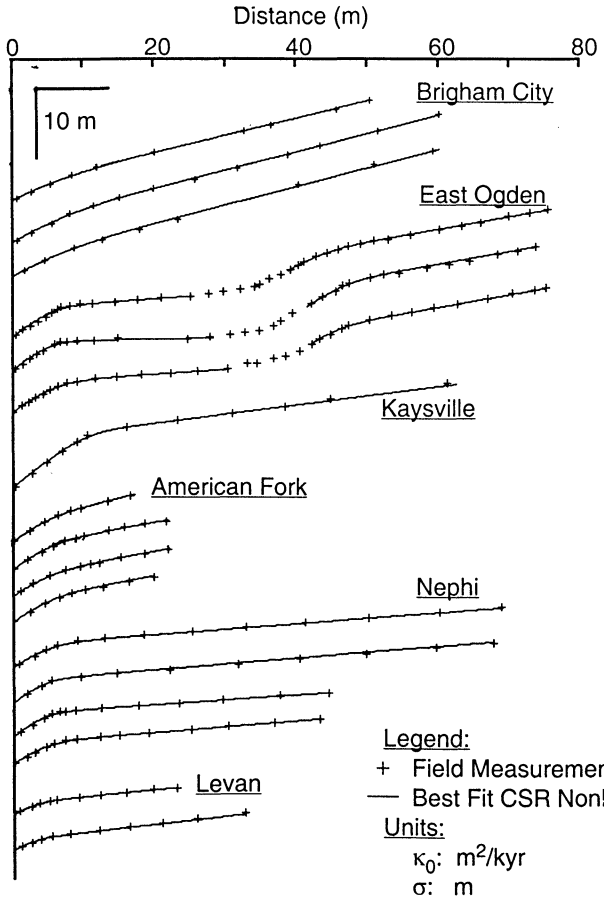

Site	κ_0	σ
Brigham City	6.1	0.041
	5.5	0.111
	5.9	0.046
East Ogden (lower)	3.2	0.162
	2.8	0.148
	4.4	0.076
East Ogden (upper)	5.3	0.082
	4.3	0.123
	3.1	0.071
Kaysville	1.5	0.156
American Fork	1.9	0.079
	2.2	0.067
	2.6	0.050
	2.3	0.062
Nephi	3.6	0.102
	2.1	0.066
	2.0	0.099
	3.0	0.177
Levan	2.1	0.062
	1.7	0.074

Figure 7. Upper half of fault scarp profiles for calibration sites along the WFZ (Table 1). The κ_0 and σ for each best fit curve are shown to the right of the profile.

Table 3. Summary of Multiple-Event Fault Scarp Calibration Sites

Site	Number of Profiles	Height, m	Time (ml*), ka	κ_0 ME, m^2/kyr	κ_0 CSR, m^2/kyr	κ CSR, m^2/kyr
Brigham City	3	5.2 ± 0.7	5.0 –7.0 (6.0)	5.2 ± 0.8	5.8 ± 0.3	14.5 ± 1.1
East Ogden	3	12.1 ± 0.4	3.5 – 4.0 (3.8)	2.3 ± 0.7	3.9 ± 1.0	7.2 ± 1.0
Kaysville	1	13.7	11 – 15 (13)	1.2	1.5	6.1
American Fork	4	5.9 ± 0.7	5.0 – 5.6 (5.3)	1.1 ± 0.3	2.3 ± 0.3	6.3 ± 0.5
Nephi	4	6.2 ± 0.3	4.0 – 4.5 (4.3)	1.8 ± 0.6	2.7 ± 0.8	5.3 ± 1.6
Levan	2	3.1	3.6 – 4.2 (3.9)	0.8	1.9	3.4
Average				2.2 ± 1.5	3.3 ± 1.5	6.9 ± 3.0
Average without Brigham City				1.7 ± 0.8	2.8 ± 1.1	6.0 ± 1.5

*Here ml is most likely age.

nonlinear solution should be used, but for small scarps ($2a < 3$ m) the linear solution should be adequate [*Andrews and Bucknam*, 1987; *Hanks and Andrews*, 1989]. For scarps formed by multiple surface-rupturing events the CSR nonlinear solution should be used. To help determine whether to use the SE or CSR solution, the characteristic offset per event for the fault can be compared to the measured scarp height [*Wells and Coppersmith*, 1994]. A change in slope on the scarp face can also indicate that a scarp is generated by multiple surface-rupturing events [*Mayer*, 1984; *Avouac and Peltzer*, 1993]. Model parameters must either be calibrated, as in this study, or estimated from previously published data.

5. Applications to Neotectonics in Utah

The diffusion equation model is a useful reconnaissance tool for neotectonic studies. We demonstrate this by estimating the slip rate for Quaternary faults at several localities in the eastern Great Basin (Figure 9) and along the WFZ (Figure 3). The CSR nonlinear solution is applied to undated, multiple-event fault scarps located on the Nephi segment of the WFZ and along the western flanks of the Oquirrh and Stansbury Mountains. We have shown that κ_0 is 1.2 ± 0.3 m^2/kyr since 17 ka based on Lake Bonneville scarps and 2.8 ± 1.1 m^2/kyr since ~10 ka based on WFZ scarps. For purposes of this study we assume that κ_0 can be extended back in time. The goal is to demonstrate that diffusion equation modeling can be used to investigate several problems including (1) evidence for temporal variations in faulting, (2) slip rate calculations for undated scarps, (3) spatial variations in slip rate along the strike of the Stansbury Mountain fault zone, and (4) spatial variations in slip rate among three eastern Great Basin fault zones.

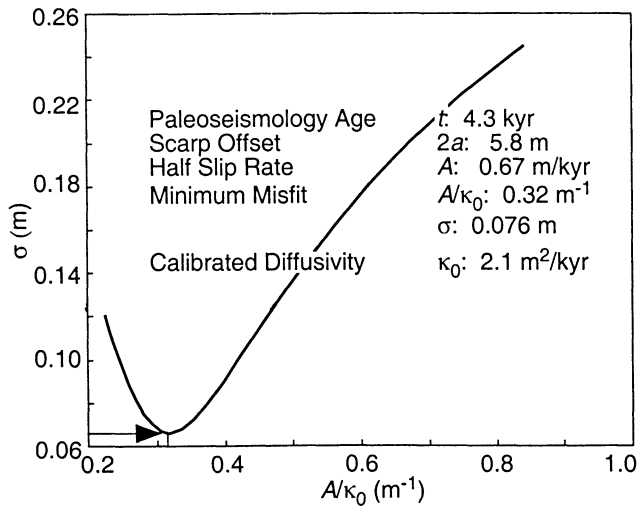

Figure 8. Plot of standard deviation as a function of A/κ_0, for a fault scarp profile near Nephi fitted with a CSR nonlinear curve. The preferred A/κ_0 solution corresponds to the minimum standard deviation. At calibration sites, t is known from paleoseismology trench data, $2a$ (scarp offset) is known from surveying, and κ_0 is determined from the preferred solution. For application sites, κ_0 is specified and A and therefore t are determined from the preferred solution.

5.1. Nephi Segment, WFZ

Quaternary fault scarps extend for ~33 km along the southern Wasatch Mountain front to form the Nephi segment of the WFZ [*Jackson*, 1991; *Harty et al.*, 1997]. Alluvial surfaces of three different ages are offset near the southern end of the segment

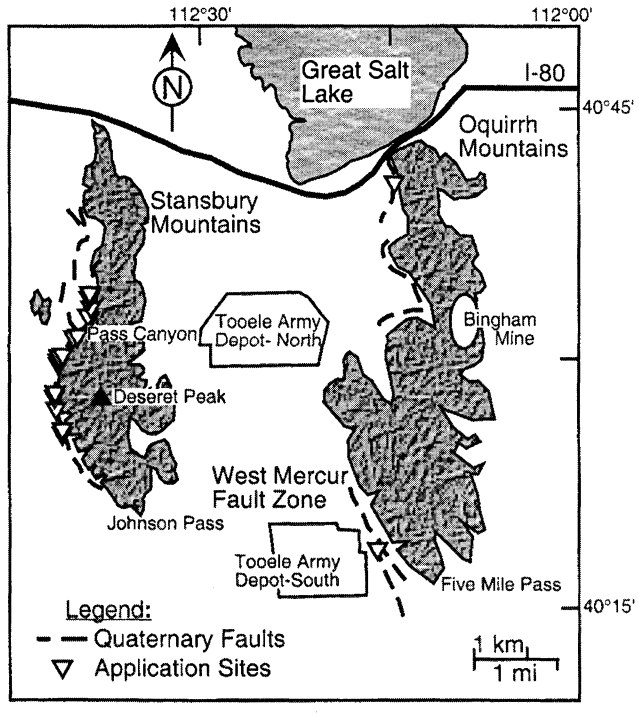

Figure 9. Location map indicating application sites for fault scarps west of the WFZ on the west flanks of the Oquirrh and Stansbury Mountains. Note the proximity of these Quaternary faults to critical U.S. Army facilities.

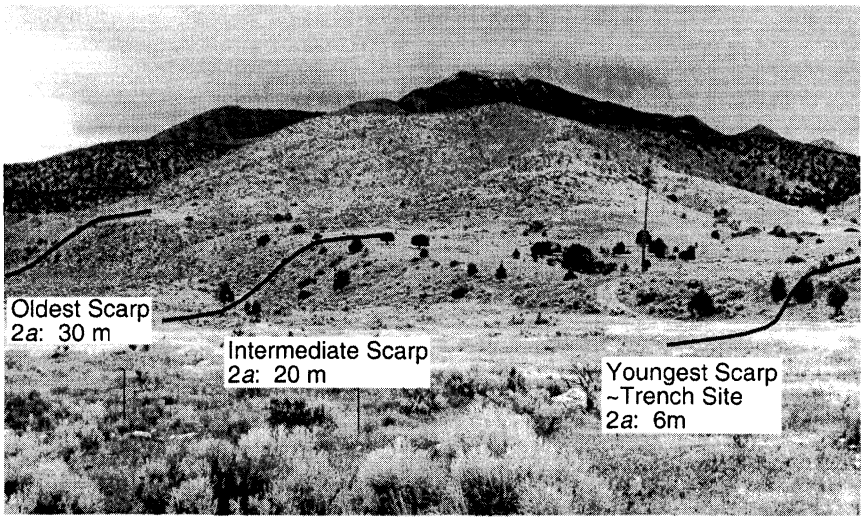

Figure 10. Photograph of a fault scarp along the Nephi segment, looking east. Paleoseismology trench site is to the right in the picture, and the older alluvial fan surfaces are to the left. The profile lines sketched on the photo indicate the approximate locations of the fault scarp profiles in Figure 11.

[*Harty et al.*, 1997], providing an opportunity to investigate variability in fault slip rate for three different time intervals at one locality (Figure 10). The scarp developed in the youngest surface is ~6 m high and is generated by three surface-rupturing events since 4.0–4.5 ka as documented in a paleoseismology trench [*Jackson*, 1991]. Scarp height increases abruptly along strike to the north where two progressively older alluvial surfaces are offset ~20 m and ~30 m, respectively. Fault scarps displacing the older surfaces are a result of the last three events recorded in the younger deposits, plus several earlier surface-rupturing events. An increase in slope near the base of the oldest scarp appears to reflect the last three events that displaced the Nephi segment (Figure 11). This steeper segment is ~6 m high, which is equal to the offset of the youngest fan surface.

Application of the CSR nonlinear model ($\kappa_0 = 2.8$ m^2/kyr; $S_c = 0.95$) to these three fault scarps indicates a possible temporal variation in slip rate. Paleoseismology trench data indicate the youngest surface began to rupture at ~4.3 ka with a slip rate of 1.3 mm/yr [*Jackson*, 1991]. Diffusion equation modeling suggests that faulting of the intermediate age surface began at ~35 ka, at a rate of 0.6 mm/yr. Faulting on the oldest surface began at ~70 ka, at a rate of 0.4 mm/yr. Therefore the slip rate from 70 ka to 4.3 ka is ~0.4 mm/yr, or ~3 times less than the slip rate estimated in the paleoseismology study. This apparent decrease in slip rate as a function of elapsed time implies either temporal clustering of earthquakes or variations in slip rate at Nephi, assuming that κ_0 remained constant. If diffusivity is doubled due to a wetter climate prior to 20 ka, then the slip rate would approximately double for that time frame but would still be less than the paleoseismology rate The steep segment at the base of the oldest (tallest) scarp suggests that temporal clustering did occur. If the fault ruptured at a regular time interval, then the tallest scarp would not preserve the change in slope reflecting the last three events because diffusion would erase each event sequentially.

Scarp	Offset, m	κ_0, m^2/kyr	Age, ka	SR, mm/yr
Oldest	27	2.8	70	0.4
Intermediate	20	2.8	35	0.6
Youngest	6	2.7	4.3	1.3

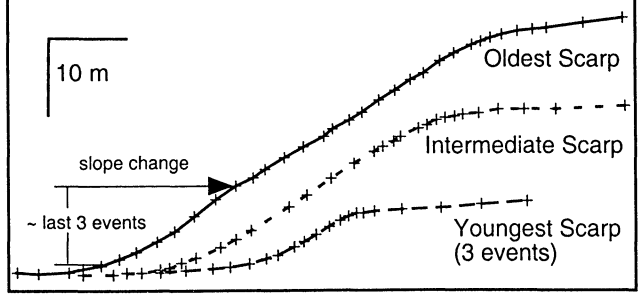

Figure 11. Comparison of three fault scarp profiles north of Nephi, Utah. The change in slope of the tallest scarp profile appears to correspond to the height of the smallest scarp profile and possibly records the last three seismic events. Analysis of these profiles suggests variation in average slip rate through time.

5.2. West Mercur Fault, Oquirrh Mountains

The West Mercur Fault (Figure 9) on the southwest flank of the Oquirrh Mountains is part of a complex zone of west dipping normal faults located ~40 km west of the WFZ [*Everitt and Kaliser*, 1980]. The proximity of this scarp to environmentally sensitive U.S. Army facilities and the Wasatch Front urban area makes it a logical focus for seismic hazard analysis [*Olig*, 1999]. The area is also the site of ongoing GPS measurements and analysis of extensional deformation in the eastern Great Basin. The bounding fault zone along the west flank of the Oquirrh Mountains appears to be composed of two segments (north ~30 km, south ~25 km). The most recent event documented by a paleoseismology trench on the north segment is 4800–7900 calendar years with a net vertical tectonic displacement of 2.2-2.7 m [*Olig et al.*, 1996]. The most recent event documented on the southern segment is 4360 ± 1220 calendar years as determined by ^{14}C cosmogenic dating of a bedrock scarp [*Handwerger et al.*, 1999]. This bedrock scarp is 14 km NW of the Mercur site.

The main splay of the West Mercur Fault ruptures the surface of a relatively fine-grained alluvial fan 1 km west of the mouth of

Table 4. The ^{10}Be / ^{26}Al Exposure Ages From Mercur Fan[a]

Sample	Measured, atoms/gm		Exposure Age, ka		Average Age, ka
	^{10}Be	^{26}Al	^{10}Be	^{26}Al	
1	1.63E+06 ± 3.36E+04	9.55E+06 ± 2.64E05	79.6 ± 1.6	79.2 ± 2.2	79.4 ± 2.7
2	1.56E+06 ± 3.27E+04	8.97E+06 ± 4.90E05	76.1 ± 1.6	74.1 ± 4.0	75.9 ± 4.4
3	4.13E+06 ± 1.08E+05	1.94E+07 ± 4.86E05	207 ± 5.5	168 ± 4.2	183 ± 28.9
4	1.44E+06 ± 3.38E+04	8.70E+06 ± 2.54E05	70.3 ± 1.6	71.8 ± 2.1	70.8 ± 2.7

[a]Read 1.63E+06 as 1.63×10^6.

Mercur Canyon. The average slope of the fan is 0.05, and a few quartzite and limestone boulders (<1 m diameter) rest on the surface. The maximum slope of the fault scarp is 0.32 (18°), and the average scarp offset is 6.0 m. Several minor splays with offsets of 1 to 3 m are mapped to the east of the main scarp, and therefore the slip rate reported here may underestimate the total slip rate.

Application of the CSR nonlinear model (κ_0 = 2.8 m^2/kyr) to four topographic profiles measured across the main splay of the fault found a slip rate of 0.12 ± 0.02 mm/yr and elapsed time since slip initiated of 55 ± 5 ka. Slip rates are also calculated by dividing the scarp offset (6.0 m) by the ages estimated from soil profiles and cosmogenic dating to corroborate the diffusion model results. The alluvial fan displaced by the West Mercur Fault has a thick carbonate soil horizon similar to soils developed on surfaces over more than 100 kyr in the eastern Great Basin [*Olig*, 1999]. The estimated age of the soil profile implies a slip rate of 0.06 mm/yr, or a factor of 2 less than the CSR results. Cosmogenic dating of four quartzite boulders collected on the upthrown fan surface indicates an exposure age for three of the boulders of 75 ± 5 ka (Table 4), or a slip rate of 0.08 mm/yr. This value generally agrees with the diffusion modeling results. These cosmogenic dates indicate the minimum age for the fan surface and that possibly 20 kyr elapsed between fan development and the onset of the most recent period of faulting. The exposure age of the fourth boulder is 183 ± 29 ka, indicating an inherited age. This boulder may originally have been exposed on one of the older alluvial fan surfaces that border the ruptured fan.

5.3. Stansbury Mountains

The Stansbury Mountains are 60 km west of the WFZ. The west side of this range is bounded by west dipping normal faults broken into two structural segments [*Helm*, 1995]. The northern segment (~20 km) is structurally complex, whereas the southern segment (~25 km) is less complex. The structural style changes abruptly at Pass Canyon, which is thought to represent the segment boundary. Little work was done in this area until recently, when a temporary low-level nuclear waste repository was proposed 10 km west of the southern fault segment.

We modeled 13 fault scarp profiles surveyed by *Helm* [1995] along the west flank of the Stansbury Mountains. Application of the nonlinear CSR model (κ_0 = 2.8 m^2/kyr, S_c = 0.95), determined slip rates of 0.04 to 0.2 mm/yr for timescales of 10 to >100 kyr. An independent estimate of slip rate calculated from a displaced basalt flow (12 Ma) is 0.07 ± 0.02 mm/yr, which is similar to the slip rate from diffusion modeling.

Several of the scarps just south of Pass Canyon appear to represent single- or at most two-event scarps based on scarp offset and diffusion equation modeling (Figure 12). The results from the SE nonlinear model (κ_0 = 1.2 m^2/kyr, S_c = 0.95) indicate a surface-rupturing event along the western flank of the Stansbury Mountains occurred at ~10 ka which postdates the Lake Bonneville flood. On the basis of CSR modeling, a second, older event likely occurred at ~40 ka.

6. Discussion

The previous examples illustrate the utility of applying nonlinear diffusion equation models in both regional and site-specific tectonic studies. However, care must be taken to choose

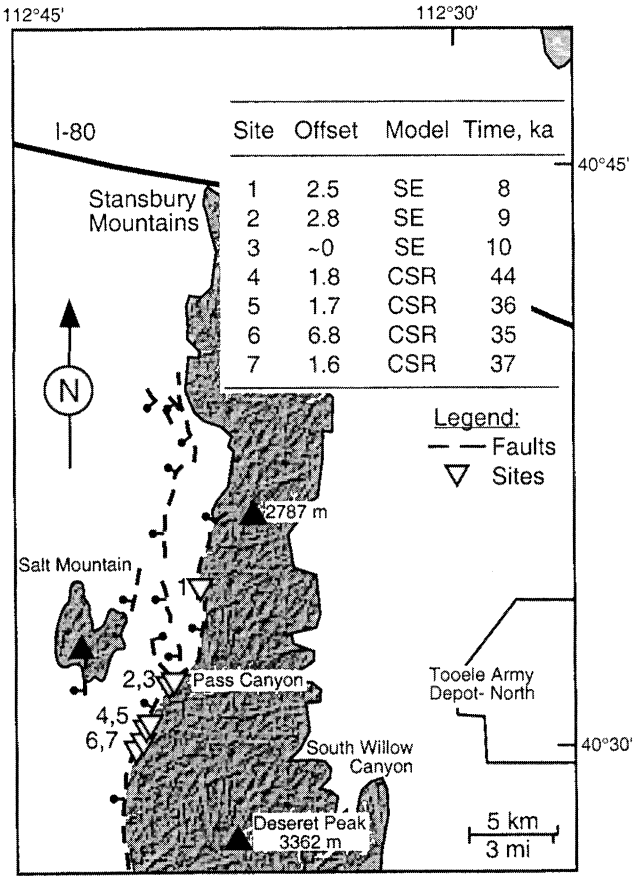

Figure 12. Location map of selected fault scarps along the northern end of the west flank of Stansbury Mountains. These scarps most likely represent one or two surface-rupturing events based on their net tectonic offset and age based on diffusion modeling. The summary table indicates the net tectonic offset, diffusion model implemented, and elapsed time (fault traces after *Helm* [1995]).

the appropriate solution for the problem at hand. The SE nonlinear solution is useful for studying scarps formed by the rapid drawdown of lakes or down cutting of fluvial channels and for dating fault scarps generated by one surface-rupturing earthquake. In this study, the CSR solution has been applied to multiple-event fault scarps where the rupture history is not known, as in site reconnaissance (Nephi, WFZ, and Oquirrh Mountains) and regional tectonic studies (Oquirrh and Stansbury Mountains).

Morphological dating has both significant advantages and limitations that should be considered when planning either a local or a regional tectonic study. The major advantage is that application of the CSR solution provides an estimate of slip rate independent of the age of the offset geomorphic surface. CSR slip rates must be more than or equal to the slip rate found by dividing scarp offset by the age of the geomorphic surface because the model predicts time elapsed since slip initiated. If the CSR slip rate is significantly higher than that calculated from the offset and age of the faulted surface, then a period of tectonic quiescence may have preceded the onset of faulting. The West Mercur Fault site may provide an example in this regard.

A significant limitation of this technique is accurate calibration of diffusivity and for the nonlinear model, S_c. S_c has a limited range of values, usually 0.75–1.0, as compared to κ_0, which can vary by an order of magnitude. Therefore κ_0 is generally the primary concern. Variations in diffusivity from site to site range by a factor of 2 along the WFZ (CSR, Levan, κ_0 = 1.9 m^2/kyr and East Ogden, κ_0 = 3.9 m^2/kyr), and variations in diffusivity from profile to profile at each site are up to 50% (CSR, Nephi, κ_0 = 2.0–3.6 m^2/kyr). The calibration process assumes that diffusivity is constant through time, but climate has changed dramatically since 100 ka due to glacial cycles that may have caused diffusivity to fluctuate. A wetter climate should increase diffusivity, and therefore our calculated slip rates for the older scarps at Nephi, Mercur, and the Stansbury Mountains may be underestimated. Soil development and vegetation may also progressively stabilize slopes and cause diffusivity to decrease through time. The nonlinear model is also more difficult to execute than the linear one because it requires the calibration of S_c in addition to κ_0.

The dependency of diffusivity on scarp height remains an important but poorly understood problem. Caution should be used when applying diffusion equation models to tall scarps (nonlinear, height >25 m). Degradation of these scarps may be dominated by nondiffusive processes such as slumping or creep as demonstrated by the North Ogden scarps or by sapping due to

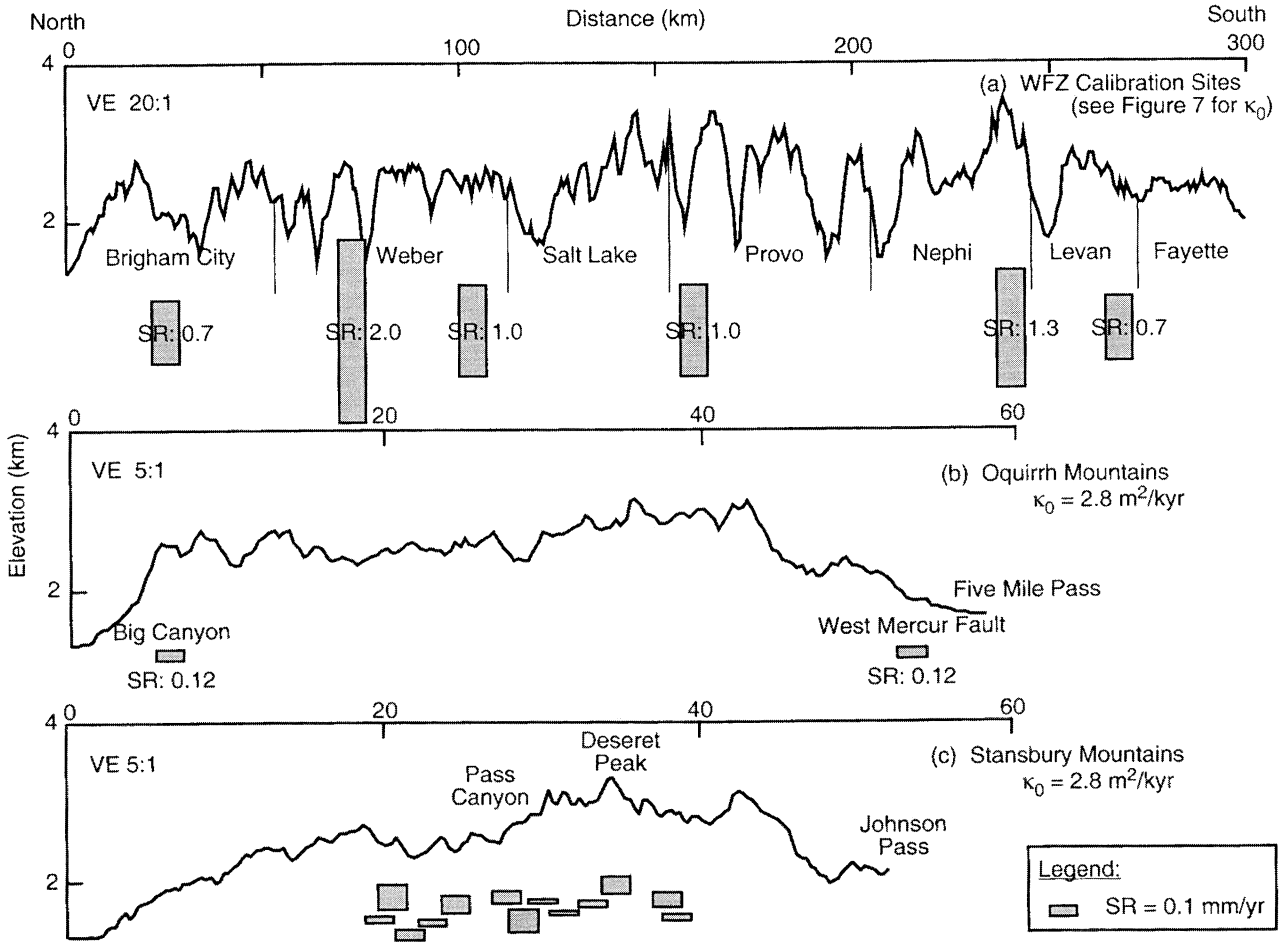

Figure 13. Average slip rates for faults along the (a) Wasatch, (b) Oquirrh, and (c) Stansbury Mountains plotted in relative north-south location against the adjacent range crest topography. The slip rates are shown as vertical bars proportional to the magnitude of the rate as determined from trench data for the WFZ and from the results of the CSR nonlinear solution for the Oquirrh and Stansbury Mountains. Diffusivity for the Oquirrh and Stansbury Mountains is assumed to be the average diffusivity of the WFZ.

an elevated water table on the upthrown side of a fault. Scarps subjected to these processes will appear to have a greater diffusivity than is predicted by diffusion modeling because sediment transport will be more rapid. The transition from diffusive processes to nondiffusive processes will probably vary regionally due to climate and aggregate properties of the sediments.

Diffusion equation modeling provides information on tectonic rates at timescales intermediate to geodetic observations and large-scale geomorphic features. Tectonic evolution for timescales of 1 Myr is reflected in the morphology of the mountain range adjacent to a bounding fault (Figure 13). The central segments of the WFZ, with their higher slip rates, are characterized by greater relief, a low degree of dissection, and linear range fronts [*Schwartz and Coppersmith,* 1984]. On the other hand, the Oquirrh and Stansbury Mountains have lower relief, a greater degree of dissection, and less linear range fronts. Geodetic measurements for timescales of <100 years, including new Global Positioning System (GPS) campaigns, indicate that extension rates are greater across the WFZ than across the Oquirrh and Stansbury Mountains [*Martinez et al.*, 1998]. Results from diffusion equation modeling also support these observations that the WFZ is more active than the other ranges in the eastern Great Basin and further point to the applicability of diffusion modeling for regional tectonic studies.

7. Conclusions

This study demonstrates that diffusion equation models can estimate the time elapsed since slip initiated on a faulted surface and therefore may estimate slip rate and relative tectonic activity more accurately than simply dividing scarp offset by the age of the ruptured surface. Diffusion equation models replicate the morphology of shoreline scarps and multiple-event fault scarps, but care must be used for scarps more than ~25 m high. Tall scarps often exhibit hummocky topography indicating that degradation may be controlled by nondiffusive processes such as slumping and creep. Offset and age data from paleoseismology trench studies can be used to calibrate diffusion equation models and generate either ME profiles based on several individual rupture events or generate CSR profiles to estimate slip rate for a surface offsetting at a constant rate. CSR profiles approximate ME profiles for the timescales of this calibration study (< 10 kyr), and therefore the CSR model is applied to undated scarps thought to represent more than one surface-rupturing event. The SE model is applied to scarps that represent a single surface-rupturing event or a sudden drawdown of a lake or river.

Diffusion equation models are used as a reconnaissance tool to estimate slip rate and temporal patterns of faulting in the eastern Great Basin. Variations in the slip rate for surfaces of different ages on the Nephi segment of the WFZ indicate the possibility of temporal clustering or variable slip rate. An increase in slope near the base of the oldest scarp at Nephi appears to reflect the offset of the youngest three events recorded in a nearby paleoseismology trench.

Application of the CSR nonlinear model indicates that slip rate decreases by up to an order of magnitude from the WFZ to the Oquirrh and Stansbury Mountains fault zones and that fault displacement is not uniform through time. Modeling the West Mercur Fault found a slip rate of ~0.1 mm/yr along the main trace, which generally agrees with the rate determined by cosmogenic dating. The observed difference between the minimum age of the ruptured surface and the time that slip initiated on the fault may indicate a period of quiescence on the fan surface. Slip rate varies along the west flank of the Stansbury Mountains, indicating differing rates of tectonic activity and a most recent surface-rupturing event at ~10 ka.

Acknowledgments. The authors wish to thank Thomas C. Hanks, USGS, for many discussions about diffusion equation modeling, reconnaissance work in the field, and review of the preliminary manuscript; Robert C. Finkel, LLNL, for providing the cosmogenic dates for the Mercur Fan; and Susan Olig, URS Greiner Woodward Clyde, for discussions and preliminary results on the West Mercur area. This work was funded in part by the University of Utah Research Committee.

References

Andrews, D.J., and R.C. Bucknam, Fitting degradation of shoreline scarps by a nonlinear diffusion model, *J. Geophys. Res.*, *92*, 12,857-12,867, 1987.

Arrowsmith, J.R., D.D. Rhodes, and D.D. Pollard, Morphologic dating of scarps formed by repeated slip events along the San Andreas Fault, Carrizo Plain, California, *J. Geophys. Res.*, *103*, 10,141-10,160, 1998.

Avouac, J.P., Analysis of scarp profiles: Evaluation of errors in morphologic dating, *J. Geophys. Res.*, *98*, 6745-6754, 1993.

Avouac, J.P., and G. Peltzer, Active tectonics in southern Xinjiang, China: Analysis of terrace riser and normal fault scarp degradation along the Hotan-Qira fault system, *J. Geophys. Res.*, *98*, 2,1773-2,1807, 1993.

Avouac, J.P., J.F. Dobremez, and L. Bourjot, Paleoclimatic interpretation of a topographic profile across middle Holocene regressive shorelines of Longmu Co (western Tibet), *Palaeogeogr. Palaeoclimatol. Palaeoecol.*, *120*, 93-104, 1996.

Bowman, D., and R. Gerson, Morphology of the latest Quaternary surface-faulting in the Gulf of Elat region, eastern Sinai, *Tectonophysics*, *128*, 97-119, 1986.

Buchun, Z., L. Yuhua, G. Shunmin, R.E. Wallace, R.C. Bucknam, and T.C. Hanks, Fault scarps related to the 1739 earthquake and seismicity of the Yinchuan graben, Ningxia Huizu Zizhiqu, China, *Bull. Seismol. Soc. Am.*, *76*, 1253-1287, 1986.

Bucknam, R.C., and R.E. Anderson, Estimation of fault-scarp ages from a scarp-height-slope angle relationship, *Geology*, *7*, 11-14, 1979.

Enzel, Y., R. Amit, N. Porat, E. Zilberman, and B.J. Harrison, Estimating the ages of fault scarps n the Arava, Israel, *Tectonophysics*, *253*, 305-317, 1996.

Everitt, B.L., and B.N. Kaliser, Geology for assessment of seismic risk in the Tooele and Rush Valleys, Tooele County, Utah, *Spec. Stud. 51*, 33 pp., Utah Geol. and Min. Surv., Salt Lake City, 1980.

Forman, S.L., and A.R. Nelson, Thermoluminescence dating of fault-scarp-derived colluvium: deciphering the timing of paleoearthquakes on the Weber Segment of the Wasatch Fault Zone, north central Utah, *J. Geophys. Res.*, *96*, 595-605, 1991.

Handwerger, D.A., T.E. Cerling, and R.L. Bruhn, Cosmogenic ^{14}C in carbonate rocks, *Geomorphology*, *27*, 13-24, 1999.

Hanks, T.C., The age of scarplike landforms from diffusion-equation analysis, in *Quaternary Geochronology: Methods and Applications*, *AGU Ref. Shelf*, vol. 4, edited by J.S. Noller, J.M. Sowers, and W.R. Lettis, pp. 313-338, AGU, Washington, D. C., 1999.

Hanks, T.C., and D.J. Andrews, Effect of far-field slope on morphologic dating of scarplike landforms, *J. Geophys. Res.*, *94*, 565-573, 1989.

Hanks, T.C., and D.P. Schwartz, Morphologic dating of the pre-1983 fault scarp on the Lost River Fault at Doublespring Pass Road, Custer County, Idaho, *Bull. Seismol. Soc. Am.*, *77*, 837-846, 1987.

Hanks, T.C., and R.E. Wallace, Morphological analysis of the Lake Lahontan shoreline and beachfront fault scarps, Pershing County, Nevada, *Bull. Seismol. Soc. Am.*, *75*, 835-846, 1985.

Hanks, T.C., R.C. Bucknam, K.R. Lajoie, and R.E. Wallace, Modification of wave-cut and faulting-controlled landforms, *J. Geophys. Res.*, *89*, 5771-5790, 1984.

Harty, K.M., W.E. Mulvey, and M.N. Machette, Surficial geologic map of the Nephi segment of the Wasatch Fault Zone, eastern Juab County, Utah, *Map 170*, scale 1:24,000, Utah Geol. Surv., Salt Lake City, 1997.

Helm, J.M., Quaternary faulting in the Stansbury fault zone, Tooele County, Utah, in *Environmental and Engineering Geology of the Wasatch Front Region,* edited by W.R. Lund, *Publ. 24,* pp. 31-44, Utah Geol. Assoc., Salt Lake City, 1995.

Jackson, M., Paleoseismology of Utah, vol. 3, Number and timing of Holocene paleoseismic events on the Nephi and Levan segments,

Wasatch Fault Zone, Utah, *Spec. Stud. 78*, 23 pp., Utah Geol. Surv., Salt Lake City, 1991.

Keller, E.A., and N. Pinter, *Active Tectonics Earthquakes, Uplift, and Landscape*, 338 pp., Prentice-Hall, Old Tappan, N. J., 1996.

Martinez, L.J., C.M. Meertens, and R.B. Smith, Rapid deformation rates along the Wasatch Fault Zone, Utah, from first GPS measurements with implications for earthquake hazard, *Geophys. Res. Lett.*, *25*, 567-570, 1998.

Mayer, L., Dating Quaternary fault scarps formed in alluvium using morphologic parameters, *Quat. Res.*, *22*, 300-313, 1984.

McCalpin, J.P., *Paleoseismology*, 588 pp., Academic, San Diego, Calif., 1996.

McCalpin, J.P., and S.P. Nishenko, Holocene paleoseismology, temporal clustering, and probabilities of future large (M>7) earthquakes on the Wasatch Fault Zone, Utah, *J. Geophys. Res.*, *101*, 6233-6253, 1996.

McCalpin, J.P., S.L. Forman, and M. Lowe, Reevaluation of Holocene faulting at the Kaysville site, Weber segment of the Wasatch Fault Zone, Utah, *Tectonics*, *13*, 1-16, 1994.

Nash, D.B., Morphologic dating of degraded normal fault scarps, *J. Geol.*, *88*, 353-360, 1980.

Nash, D.B., Morphologic dating of fluvial terrace scarps and fault scarps near West Yellowstone, Montana, *Geol. Soc. Am. Bull.*, *95*, 1413-1424, 1984.

Olig, S.S., Mapping and quaternary fault scarp analysis of the Mercur and West Eagle Hill Faults, Wasatch Front, Utah, *NEHRP 1434-HQ-97-GR-03154,* 36 pp. (without appendices), URS Greiner Woodward Clyde, Oakland, Calif., 1999.

Olig, S.S., W.R. Lund, B.D. Black, and B.H. Mayes, Paleoseismic investigation of the Oquirrh Fault Zone, Tooele County, Utah, in *The Oquirrh Fault Zone, Tooele County, Utah: Surficial Geology and Paleoseismology,* edited by W.R. Lund, *Spec. Stud. 88,* pp. 22-64, Utah Geol. Surv., Salt Lake City, 1996.

Personius, S.F., Paleoseismology of Utah, vol. 2, Paleoseismic analysis of the Wasatch Fault Zone at the Brigham City trench site, Brigham City, Utah and Pole Patch trench site, Pleasant View, Utah, *Spec. Stud. 76*, 39 pp., Utah Geol. Surv., Salt Lake City, 1991.

Pierce, K.L., and S.M. Colman, Effect of height and orientation (microclimate) on geomorphic degradation rates and processes, late-glacial terrace scarps in central Idaho, *Geol. Soc. Am. Bull.*, *97*, 869-885, 1986.

Roering, J.J., J.W. Kirchner, and W.E. Dietrich, Evidence for nonlinear, diffusive sediment transport on hillslopes and implications for landscape morphology, *Water Resour. Res.*, *35*, 853-870, 1999.

Schwartz, D.P., and K.J. Coppersmith, Fault behavior and characteristic earthquakes: Examples from the Wasatch and San Andreas fault zones, *J. Geophys. Res.*, *89*, 5681-5698, 1984.

Tapponnier, P., et al., Active thrusting and folding in the Qilian Shan, and decoupling between upper crust and mantle in northeastern Tibet, *Earth Planet. Sci. Lett.*, *97*, 382-403, 1990.

Terzaghi, K., Mechanism of landslides, in *Application of Geology to Engineering Practice*, edited by S. Paige, pp. 83-123, Geol. Soc. of Am., Boulder, Colo., 1950.

Wells, D.L., and K.J. Coppersmith, New empirical relationships among magnitude, rupture length, rupture width, rupture area, and surface displacement, *Bull. Seismol. Soc. Am.*, *84*, 974-1002, 1994.

R. L. Bruhn and A. Mattson, Department of Geology and Geophysics, University of Utah, 135 S. 1460 East, Rm. 719, Salt Lake City, UT 84112. (rlbruhn@mines.utah.edu; amattson@mines.utah.edu)

(Received May 18, 2000; revised December 12, 2000;
accepted December 22, 2000)